Supporting Information

Promoting the Formation of Metal-Carboxylate Coordination to Modulate the Dimensionality of Ultrastable Lead Halide Hybrids

*Yilin Jiang, Jinlin Yin, Ruonan Xi, and Honghan Fei**

School of Chemical Science and Engineering, Shanghai Key Laboratory of Chemical Assessment and Sustainability, Tongji University, Shanghai 200092, P. R. China

Corresponding Author: fei@tongji.edu.cn

Experimental Section

Materials. All starting reagents, materials and solvents were purchased from commercial supplier and used without further purification. Lead chloride ($PbCl_2$, 99.0%, Aladdin), lead bromide ($PbBr_2$, 99.0%, Aladdin), 1,4-cyclohexanedicarboxylate ($C_8H_{12}O_4$, >98.0%, Adamas), 1,2,4,5-cyclohexanetetracarboxylate ($C_{10}H_{12}O_8$, >97.0%, Bide Pharmatech), 1,2,3,4,5,6-cycloexanehexacarboxylate ($C_{12}H_{12}O_{12}\cdot H_2O$, >97.0%, Aladdin), acetonitrile (CH_3CN, >99.0%, Greagent), ethanol (EtOH, >99.5%, Greagent), methanol (MeOH, >99.5%, Greagent), ethylbenzene (99%, Adamas), naphthalene (99%, Adamas), potassium tetrachloroplatinate (K_2PtCl_4, 98%, Adamas), and deionized water was obtained from a BARNSTEAD PACIFIC RO water purification system.

Synthesis of TJU-13(Cl). A mixture of 0.334 g $PbCl_2$ (1.2 mmol), 0.156 g 1,2,4,5-cyclohexanetetracarboxylate (0.6 mmol), and 10 mL solvents of H_2O/MeCN (2:1 v:v) were added into a 15 mL Teflon-lined autoclave, followed by 15 min stirring for sufficient dispersion. The autoclave was then sealed into a stainless-steel vessel and heated statically at 120 °C for 72 h. Upon the autoclave cooling to room temperature, the colorless block-shaped crystals were isolated by vacuum filtration, rinsed with ethanol, and then dried at 60°C for 10 h (yield: 325 mg, ~81% based on Pb). Element analysis: calculated C, 12.01%; H, 1.37%; found C, 11.97%; H, 1.40%.

Synthesis of TJU-13(Br). Colorless crystal TJU-13(Br) can be synthesized in the same manner as for TJU-13(Cl) but with $PbBr_2$ in place of $PbCl_2$. (yield: 371 mg, ~85% based on Pb). Element analysis: calculated C, 11.02%; H, 1.25%; found C, 10.99%; H, 1.28%.

Synthesis of TJU-14(Cl). A mixture of 0.348 g $PbCl_2$ (1.25 mmol), 0.092 g 1,2,3,4,5,6-cycloexanehexacarboxylate (0.25 mmol), and 10 mL solvents of H_2O were added into a 15 mL Teflon-lined autoclave, followed by 15 min stirring for sufficient dispersion. The autoclave was then sealed into a stainless-steel vessel and heated statically at 150 °C for 72 h. Upon the autoclave cooling to room temperature, the block-shaped crystals were isolated by vacuum filtration, rinsed with ethanol, and then dried at 60°C for 10 h (yield: 277 mg, ~77% based on Pb). Element analysis: calculated C, 4.25%; H, 0.23%; found C, 4.18%; H, 0.20%.

Synthesis of TJU-15(Br). Colorless crystal TJU-15(Br) can be synthesized in the same manner as for TJU-14(Cl) but with $PbBr_2$ in place of $PbCl_2$. (yield: 335 mg, ~75% based on Pb). Element analysis: calculated C, 2.65%; H, 0.13%; found C, 2.68%; H, 0.11%.

Photodeposition of Pt Co-catalyst. Pt nanoparticles were photodeposited onto the as-synthesized photocatalysts by using K_2PtCl_4 as the metal precursor. Specifically, 20 mg of photocatalysts in the form of microcrystalline powders were first dispersed in a mixed solution of 1.5 mL H_2O and 1.5 mL methanol containing a specific amount of the metal precursor (Table S4). The mixture was then irradiated by an UV lamp for 60 min. After that, the solids were isolated by centrifugation, washed with water and ethanol for three times, and dried at 60 °C in ambient condition for 24 h.

Materials Characterization. Powder X-ray diffraction (PXRD) analysis were collected on a Bruker D2 Phaser X-ray diffractometer equipped with a Cu sealed tube (λ = 1.54184 Å) at 30 kV and 10 mA with a scan speed of 1 sec/step, a step size of 0.02° in 2θ, and a 2θ range of 5–40°. Element analysis (EA) for C/H were performed in a Varian EL III element analyzer. Thermogravimetry analysis (TGA) was carried out on a TGA Q5000 differential thermal analyzer. The samples were heated in a N_2 stream from room temperature to 800 °C with a heating rate of 10 °C/min. Ultraviolet-visible (UV-Vis) diffusion reflectance spectroscopy was performed on an Agilent Carry 5000 spectrophotometer equipped with an integrating sphere, using 100% $BaSO_4$ as reflectance standard for all measurements. Metallic elemental contents for Pt were measured on a Perkin Elmer Optima 8300 ICP-OES. Scanning electron microscopy and elemental mapping of energy-dispersive X-ray spectroscopy (EDS) were carried out on a Hitachi S4800 field-emission scanning electron microscopy (FE-SEM) equipped with EDS. High-resolution transmission electron microscopy (HRTEM) were performed using a JEOL 2010 microscope operated at 200 kV. UV photoelectron spectra (UPS) were collected by a Shimadu/Kratos Axis Supra spectrometer with He I radiation (21.22 eV). The steady photoluminescence spectra were recorded on a Horiba Fluorolog setup in reflection geometry (Fluorolog-3-11). Femtosecond TA spectroscopy was performed on a Helios pump–probe system (Ultrafast Systems LLC) combined with an amplified femtosecond laser system (Coherent), by dispersion of samples powders in ethylene glycol. Electron paramagnetic resonance (EPR) spectra were obtained over JES-FA200

electron paramagnetic resonance spectrometer (JEOL) with 5,5-dimethyl-1-pyrroline-N-oxide (DMPO) as spin trap.

Single Crystal X-ray Diffraction (SCXRD). The crystal structure data were collected on a BRUKER D8 VENTURE diffractometer equipped with a PHOTON III detector. Diffraction data were processed with the APEX3 software package, integrated using SAINT, and further corrected for absorption effects using SADABS. Space groups were determined by systematic absences, E-statistics, agreement factors for equivalent reflections, and successful refinement of the structure. The structures were solved by direct methods and expanded routinely, and refined by full-matrix least-squares analysis of F^2 against all reflections using SHELXTL software package. All non-hydrogen atoms were refined with anisotropic thermal displacement parameters. Thermal parameters for hydrogen atoms were tied to the isotropic thermal parameter of the atoms to which they are bonded.

AC Hall Measurement. Hall effect measurements were carried out on an Accent HL5500 Hall system, in which the manually grounded powder samples were first pressed into tablets of ~1.5 cm in diameter, and then four electrodes were soldered to each corner. The magnetic field for the test is 0.5 T and the range of test current was from 10 nA to 1 mA. The Hall system used a rotating parallel dipole line magnet that generates AC field with pure harmonic, unidirectional, and strong magnetic field followed by Fourier spectral analysis and lock-in detection of the Hall signal.

Time-Resolved Photoluminescence. Time-resolved emission data was collected at room temperature using an EDINBURGH FLS980 steady state/transient state fluorescence/phosphorescent spectrometer equipped with time-correlated single photon counting (TCSPC) system. The average lifetime was obtained according to the equation:

$$\tau_{\mathrm{avg}} = \frac{\sum \alpha_{\mathrm{i}} \tau_{\mathrm{i}}^2}{\sum \alpha_{\mathrm{i}} \tau_{\mathrm{i}}} \quad i = 1,2,3\ldots$$

where a_i represents the amplitude of each component and τ_i represents their decay time.

Photoelectrochemical Measurement. The photocurrent responses and electrochemical impedance spectroscopy measurements were carried out on a CHI 760E electrochemical workstation (Shanghai Chenhua) equipped with a standard three-

electrode system, including an indium-tin oxide (ITO) deposited with samples as the working electrode, an Ag/AgCl (KCl saturated) reference electrode and a Pt counter electrode. A 0.5 M Na_2SO_4 aqueous solution was used as the electrolyte. The working electrodes were prepared as follows: 10 mg of the photocatalyst samples were dispersed in a mixed solution of H_2O (1 mL), methanol (1 mL) and Nafion (10 μL) by sonication, and 100 μL of the above mixtures was coated on one side of ITO electrode followed by drying at room temperature. The frequency range was measured from 1 Hz to 1 MHz. In the photocurrent measurements, a 300 W Xenon lamp with the AM 1.5G filter was served as the incident light.

Photocatalytic Ethylbenzene Oxidation. All photocatalytic reactions were conducted in a 50 mL Pyrex top-irradiation-type reactor and with a magnetic stirring rod (500 rpm). Typically, 20 mg photocatalyst was dispersed in a mixed solution of 2 ml ethylbenzene and 1 ml acetonitrile. Before the test, the system was degassed to remove all of gases, and refilled with O_2. Then the reaction was carried out under visible light originated from a 300W Xenon lamp equipped with AM1.5G filter, and the temperature was maintained at 293K by recirculating cooling water system. After the reaction, the product was taken out from the reaction system and the conversions were checked by gas chromatography-mass spectrometry (GC-MS, Shimadzu GCMS-QP2010 SE) using naphthalene as the internal standard. The recyclability of the catalyst was tested by separation of catalysts by centrifugation, washing with ethanol and drying at 80 ℃. The active species trapping experiments were conducted by adding 0.5 mmol different types of radical scavengers (general reaction condition, 4 h) was used to understand the role of radical species involved in the photocatalytic oxidation of ethylbenzene. Tetra-methylpiperidine *N*-oxide (TEMPO) as radical scavenger, and ammonium oxalate ($(NH_4)_2C_2O_4$), benzoquinone (BQ), potassium persulfate ($K_2S_2O_8$), tert-butyl alcohol (TBA) and butylated hydroxytoluene (BHT) as scavengers for photogenerated holes, superoxide radicals, photogenerated electrons, hydroxyl radicals and carbon-centered radicals, respectively.

Chemical and Thermal Stability Studies. ~100 mg of the as-synthesized materials

were incubated in aqueous conditions (a HCl solution of pH=4 and a NaOH solution of pH=10), respectively. The samples were incubated into the above conditions for 24 h before performing PXRD. Thermal stability experiments were carried out by as-synthesized materials in oven at the corresponding temperature in air for 24 h. PXRD characterization were performed after cooling to the room temperature.

Computational Methods. The band structure and the projected density of states (PDOS) of TJU-14(Cl) and TJU-15(Br) were calculated by density functional theory method (DFT) implemented in the Vienna Ab initio Simulation Package (VASP)[S1] with the projector augmented wave (PAW) method.[S2] The Perdew-Burke-Ernzerhof (PBE) functional[S3] was employed to perform structure optimization and electronic property calculations. A cutoff energy of 450 eV was selected for the plane-wave basis. During the optimization, the cell and atomic positions were fully allowed to relax. The Brillouin zone was sampled with a Gamma-centered 2×2×2 K-point. The convergence energy threshold was set to 10^{-6} eV and the force on each atom is should within 0.01 eV/Å.

Photocatalytic Ethylbenzene Oxidation Mechanism:[S4, S5]

Initiating:

$$\text{Photocatalyst} + h\nu \rightarrow \text{h}^+ + \text{e}^-$$

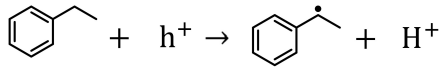

$$\cdot O_2^- + \text{h}^+ \rightarrow \text{HOO}\cdot$$

$$O_2 + \text{e}^- \rightarrow \cdot O_2^-$$

Propagating:

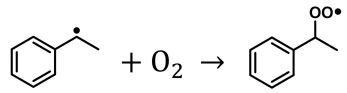

Terminating:

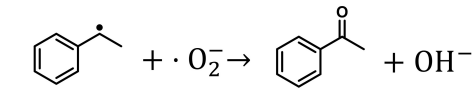

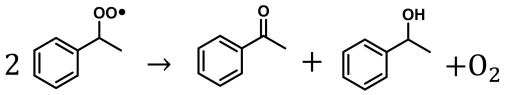

Supporting Tables and Figures

Table S1. Crystallographic data and structure refinement for TJU-13(Cl) and TJU-13(Br).

Identification code	TJU-13(Cl)	TJU-13(Br)
Empirical formula	$C_{10}H_{14}Cl_2O_{11}Pb_3$	$C_{10}H_{14}Br_2O_{11}Pb_3$
Formula weight	1002.68	1091.60
Temperature (K)	287.0	296.15
Crystal system	monoclinic	monoclinic
Space group	$P2_1/c$	$P2_1/c$
Unit cell dimensions	a=13.450(8) Å b=14.206(7) Å c=9.152(4) Å α=90° β=90.28°(2) γ=90°	a=13.6110(7) Å b=14.2371(8) Å c=9.2448(5) Å α=90° β=90° γ=90°
Volume/Å^3, Z	1748.6(16), 4	1791.47(17), 4
ρ_{calc}g/cm^3	3.809	4.047
θ range (deg)	5.296 to 55.216	5.254 to 55.034
Index ranges	$-17 \le h \le 17$ $-18 \le k \le 18$ $-11 \le l \le 11$	$-17 \le h \le 17$ $-18 \le k \le 18$ $-12 \le l \le 11$
Reflections collected	20852	22220
Independent reflections	3997 [R_{int} = 0.0560, R_{sigma} = 0.0423]	4113 [R_{int} = 0.0919, R_{sigma} = 0.0532]
Data/restraints/parameters	3997/172/245	4113/54/242
Goodness-of-fit on F^2	1.104	1.082
Final R indexes [I>=2σ (I)]	R_1 = 0.0592, wR_2 = 0.1777	R_1 = 0.0454, wR_2 = 0.1208
Final R indexes [all data]	R_1 = 0.0632, wR_2 = 0.1821	R_1 = 0.0486, wR_2 = 0.1232
Largest diff. peak/hole (e Å^{-3})	6.31/-5.05	3.07/-4.31

$R_1=\sum(||F_o|-|F_c||) / \sum|F_o|$; $wR_2=\{\sum[w(F_o^2-F_c^2)]/\sum[w(F_o^2)]^2\}^{1/2}$

Table S2. Crystallographic data and structure refinement for TJU-14(Cl) and TJU-15(Br).

Identification code	TJU-14(Cl)	TJU-15(Br)
Empirical formula	$C_{12}H_7Cl_{17}O_{13}Pb_{12}$	$C_8H_4Br_{16}O_8Pb_{10}$
Formula weight	3448.04	3578.57
Temperature (K)	288.0	286.0
Crystal system	trigonal	cubic
Space group	*P*-3*c*1	*Pa*-3
Unit cell dimensions	*a*=12.596(3) Å *b*=12.596(3) Å *c*=16.741(7) Å *α*=90° *β*=90° *γ*=120°	*a*=18.621(8) Å *b*=18.621(8) Å *c*=18.621(8) Å *α*=90° *β*=90° *γ*=90°
Volume/Å^3, Z	2300(15), 2	6457(8), 6
ρ_{calc}g/cm^3	4.978	5.522
θ range (deg)	6.134 to 50.012	4.892 to 50.74
Index ranges	-14 ≤ *h* ≤ 14 -14 ≤ *k* ≤ 14 -19 ≤ *l* ≤ 19	-22 ≤ *h* ≤ 22 -22 ≤ *k* ≤ 22 -22 ≤ *l* ≤ 22
Reflections collected	35474	68217
Independent reflections	1352 [R_{int} = 0.0622, R_{sigma} = 0.0167]	1982 [R_{int} = 0.1387, R_{sigma} = 0.0308]
Data/restraints/parameters	1352/0/85	1982/0/96
Goodness-of-fit on F^2	1.133	1.088
Final R indexes [I>=2σ (I)]	R_1 = 0.0325, wR_2 = 0.0824	R_1 = 0.0431, wR_2 = 0.1133
Final R indexes [all data]	R_1 = 0.0352, wR_2 = 0.0845	R_1 = 0.0563, wR_2 = 0.1217
Largest diff. peak/hole (e Å^{-3})	2.78/-2.96	2.35/-1.71

$R_1=\sum(||F_o|-|F_c||) / \sum|F_o|$; $wR_2=\{\sum[w(F_o^2-F_c^2)]/\sum[w(F_o^2)]^2\}^{1/2}$

Table S3. Comparison of photocatalytic ethylbenzene oxidation activity.

Samples	Products rate (μmol g^{-1} h^{-1})		acetophenone selectivity (%)
	1-phenylethanol	acetophenone	
$PbBr_2$	88	33	27
TJU-11(Br)	52	112	68
TJU-13(Br)	64	115	64
TJU-15(Br)	81	164	67
$Pt_{0.43}$@TJU-11(Br)	71	133	65
$Pt_{0.35}$@TJU-13(Br)	73	163	69
$Pt_{0.44}$@TJU-15(Br)	128	198	61
$Pt_{0.66}$@TJU-15(Br)	193	305	61
$Pt_{0.84}$@TJU-15(Br)	103	166	62

Reaction conditions: photocatalyst (0.02 g), 2 mL ethylbenzene and 1 mL CH_3CN, 1 atm oxygen, 293 K, AM1.5G simulated light irradiation and irradiation time (4 h).

Table S4. Synthetic conditions and the observed Pt wt% in the final product.

Samples	Precursor mass ratio (photocatalyst:Pt)	Observed Pt wt% in catalysts by ICP-OES
$Pt_{0.43}$@TJU-11(Br)	100:0.5	0.43
$Pt_{0.35}$@TJU-13(Br)	100:0.5	0.35
$Pt_{0.44}$@TJU-15(Br)	100:0.5	0.44
$Pt_{0.66}$@TJU-15(Br)	100:1	0.66
$Pt_{0.84}$@TJU-15(Br)	100:1.5	0.84

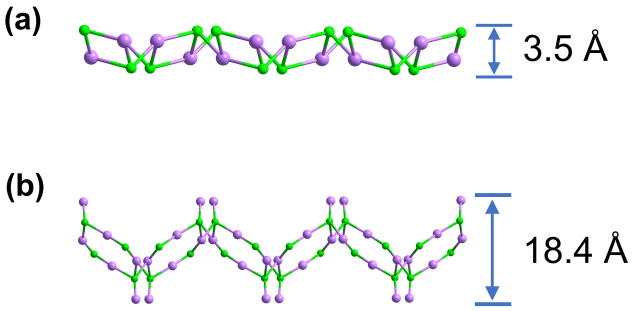

Figure S1. Layer corrugation of a single $[Pb_2Cl_2]^{2+}$ layer in TJU-10(Cl) (a) and a single $[Pb_3Cl_2]^{4+}$ layer in TJU-13(Cl) (b).

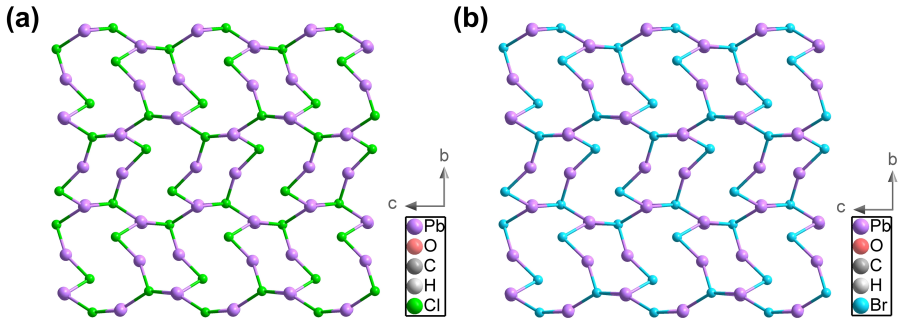

Figure S2. Crystallographic top view of a single $[Pb_3X_2]^{4+}$ (X=Cl^-/Br^-) layer in TJU-13(Cl) (a) and TJU-13(Br) (b) along the *bc* plane.

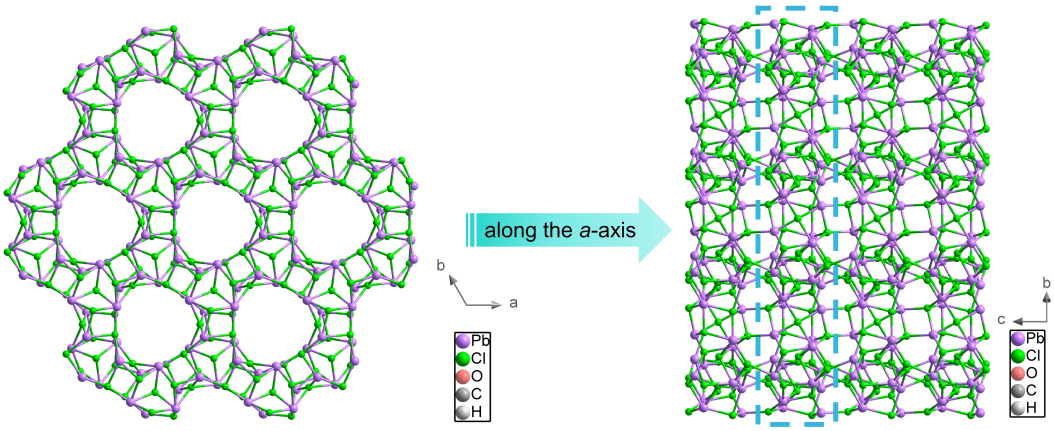

Figure S3. An array of honeycomb-like channels connected by interlamellar Pb–Cl bonds extending in three dimensions to define the 3D inorganic $[Pb_{12}Cl_{17}(OH)]^{6+}$ framework.

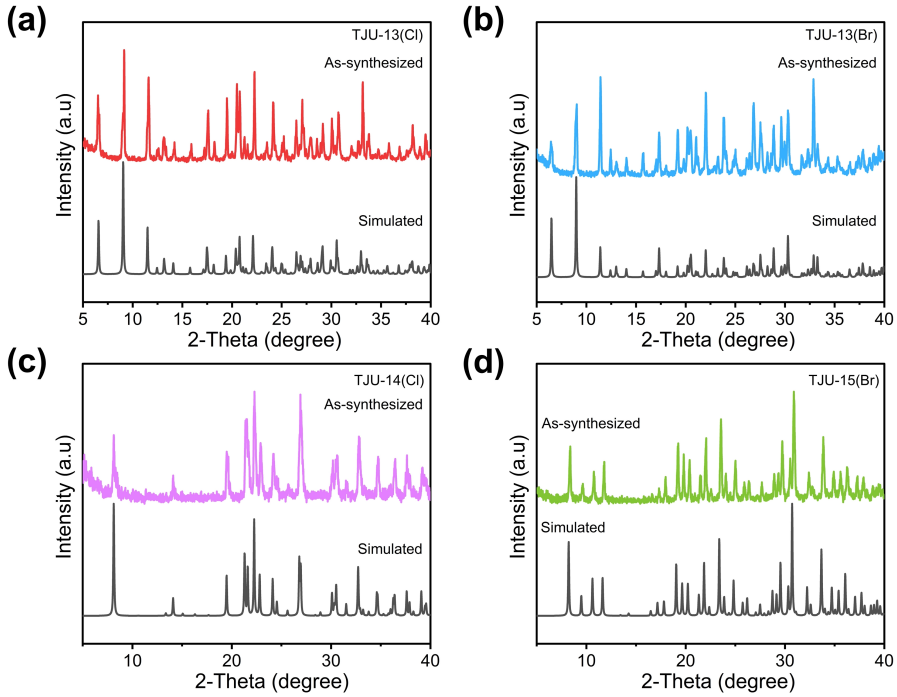

Figure S4. Simulated and experimental PXRD of TJU-13(Cl) (a), TJU-13(Br) (b), TJU-14(Cl) (c) and TJU-15(Br) (d).

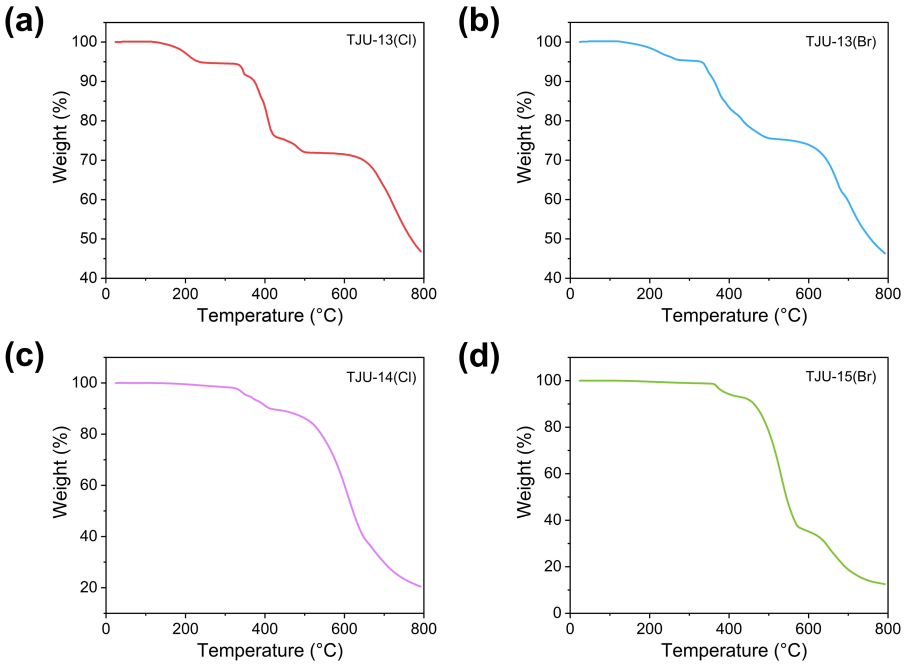

Figure S5. Thermogravimetric analysis of TJU-13(Cl) (a), TJU-13(Br) (b), TJU-14(Cl) (c) and TJU-15(Br) (d) in N_2 flow.

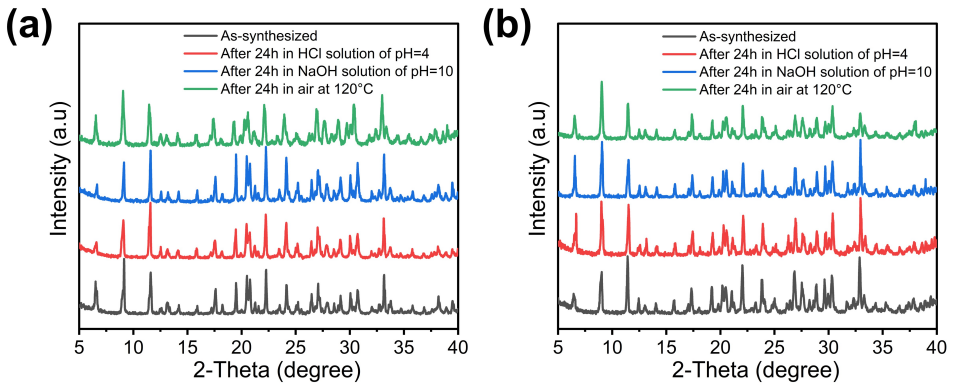

Figure S6. PXRD of TJU-13(Cl) (a) and TJU-13(Br) (b) before and after chemical treatment.

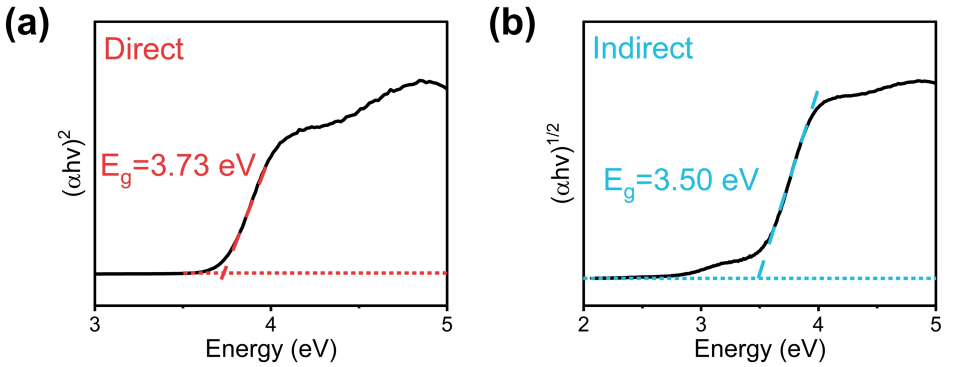

Figure S7. Tauc plot of TJU-14(Cl) fitted by direct (a) and indirect bandgap (b).

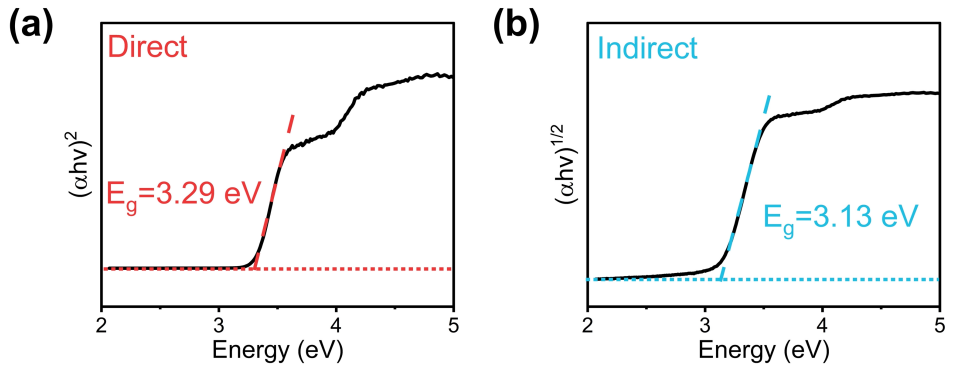

Figure S8. Tauc plot of TJU-15(Br) fitted by direct (a) and indirect bandgap (b).

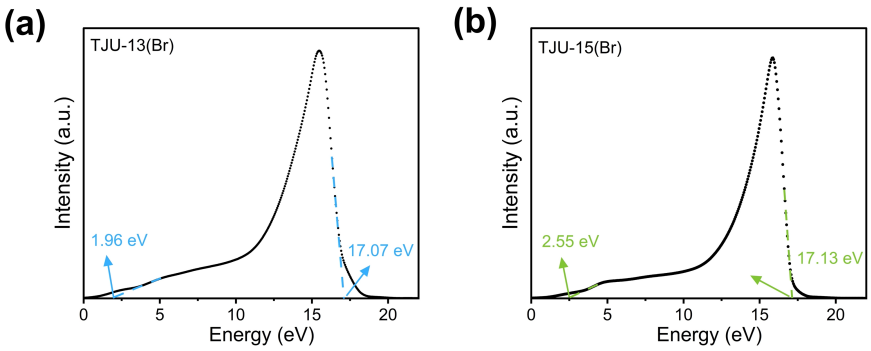

Figure S9. Ultraviolet photoelectron spectroscopy of TJU-13(Br) (a) and TJU-15(Br) (b).

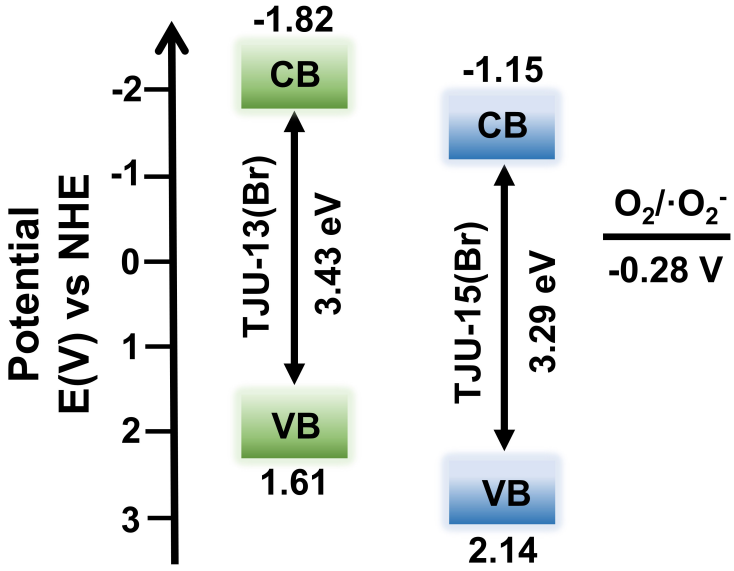

Figure S10. Band alignment of TJU-13(Br) and TJU-15(Br).

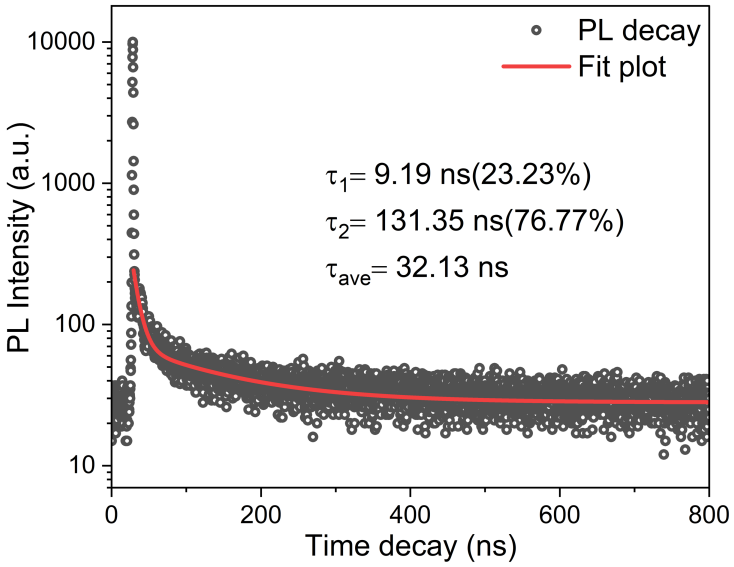

Figure S11. Photoluminescence decay curve and fitting plot of TJU-13(Br).

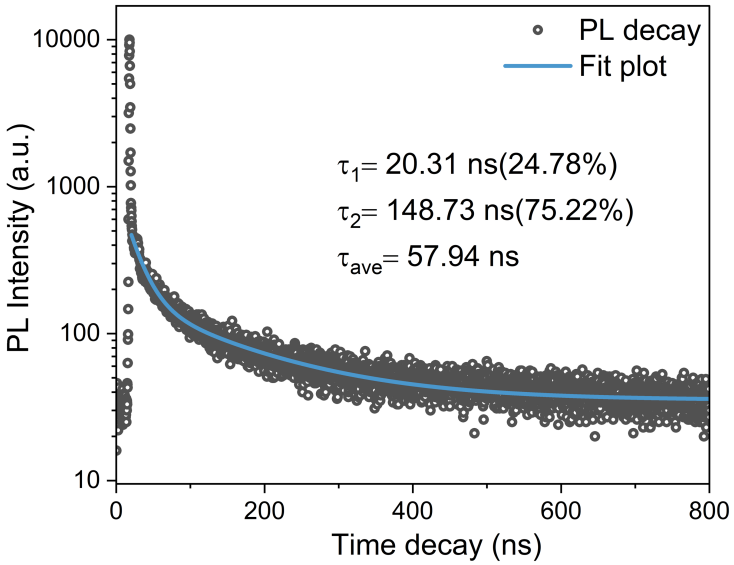

Figure S12. Photoluminescence decay curve and fitting plot of TJU-15(Br).

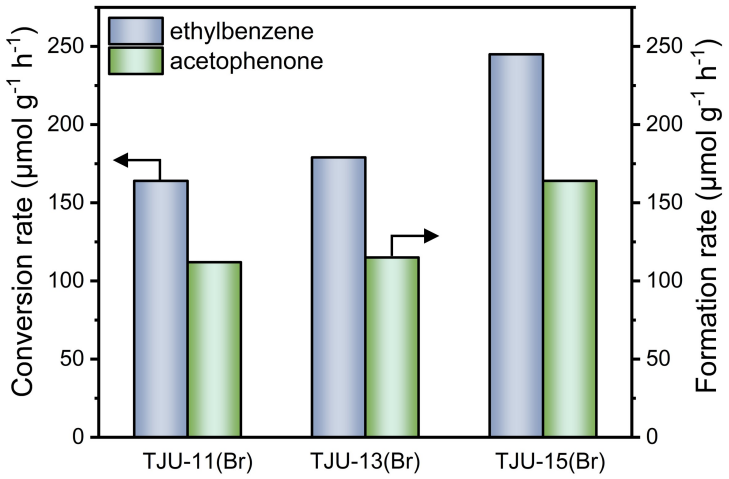

Figure S13. Conversion rates of ethylbenzene and the formation rates of acetophenone for TJU-11(Br), TJU-13(Br) and TJU-15(Br). Conditions: photocatalyst (0.02 g), 2 mL ethylbenzene and 1 mL CH_3CN, 1 atm O_2, 293 K, AM1.5G simulated light irradiation, reaction time: 4 h.

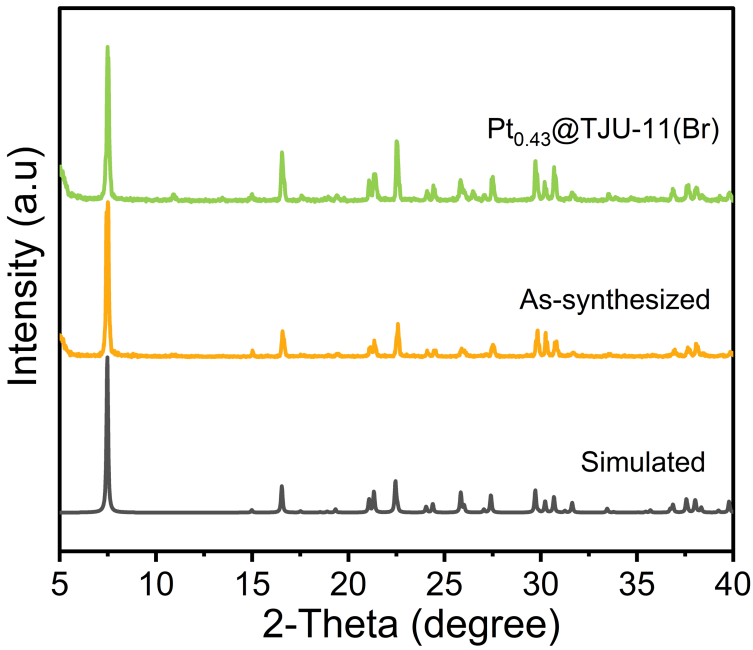

Figure S14. PXRD of $Pt_{0.43}$@TJU-11(Br) and TJU-11(Br).

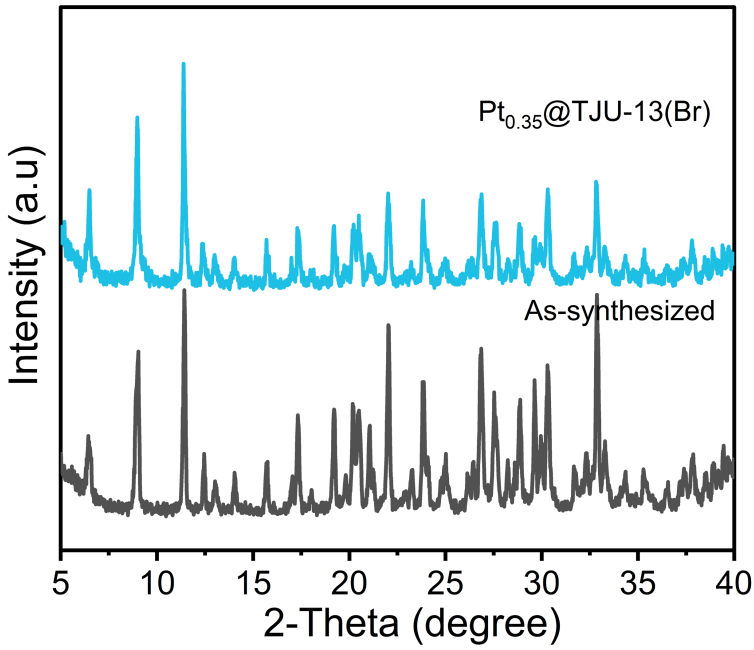

Figure S15. PXRD of $Pt_{0.35}$@TJU-13(Br) and TJU-13(Br).

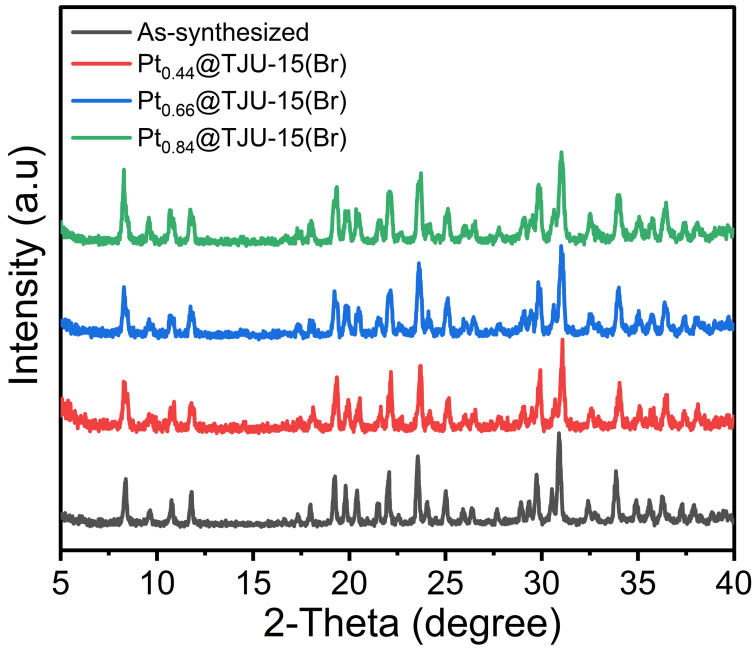

Figure S16. PXRD of Pt@TJU-15(Br) and TJU-15(Br).

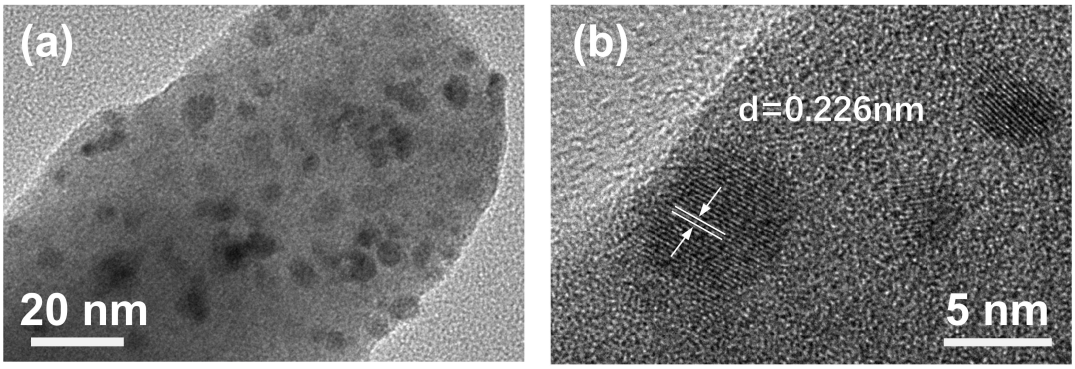

Figure S17. TEM image (a) and HRTEM image (b) of $Pt_{0.66}$@TJU-15(Br).

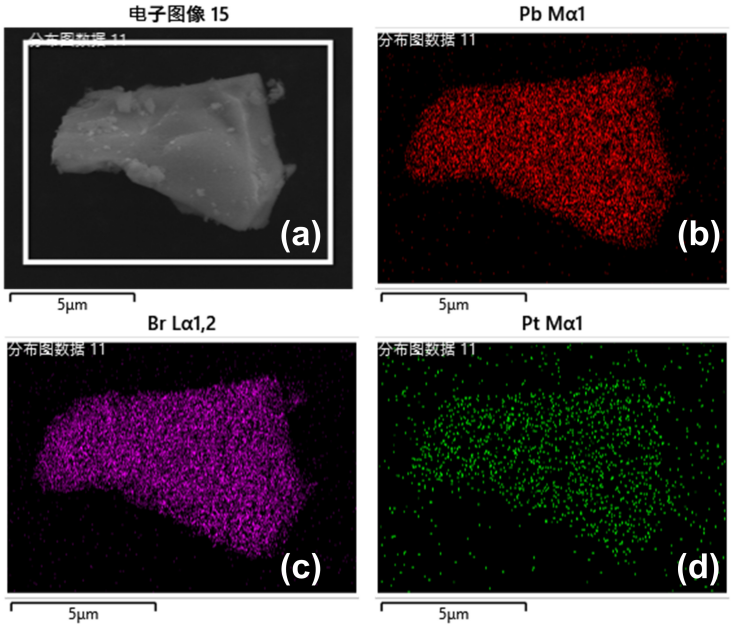

Figure S18. Pb, Br and Pt EDS mapping of $Pt_{0.66}$@TJU-15(Br).

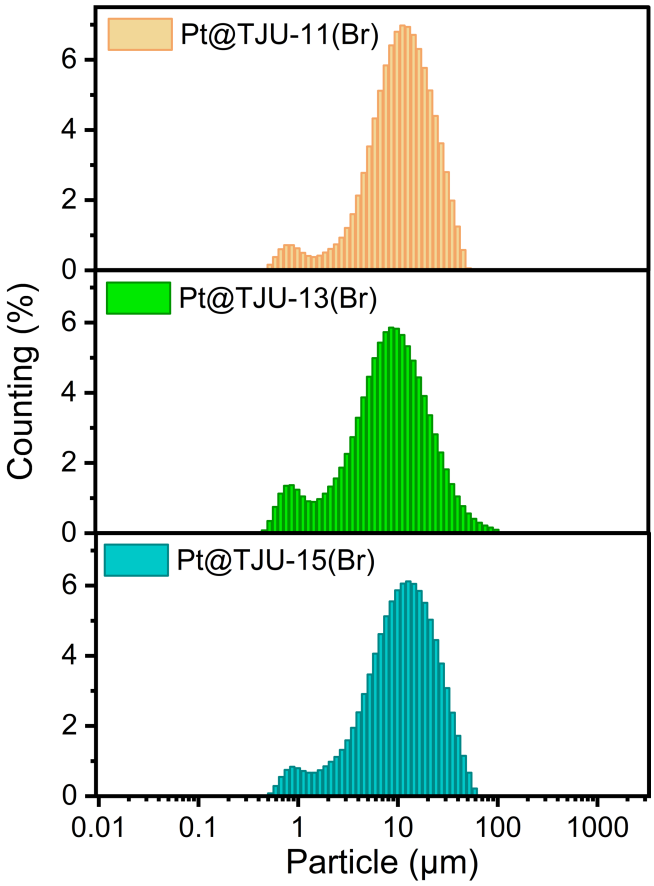

Figure S19. Particle size distribution of Pt@TJU-11(Br), Pt@TJU-13(Br) and Pt@TJU-15(Br).

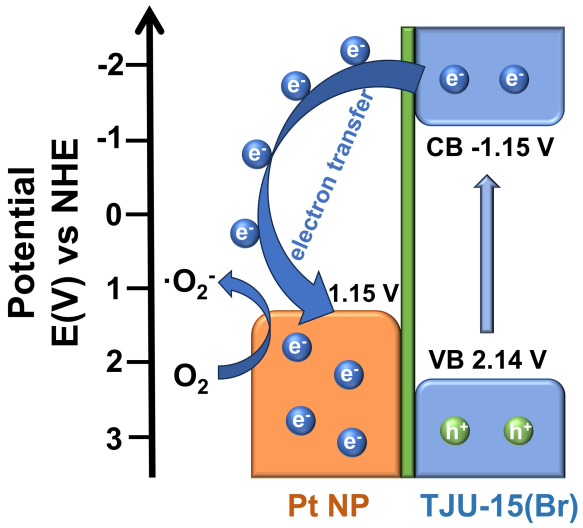

Figure S20. Schematic illustration showing the electron transfer process between TJU-15(Br) and deposited Pt nanoparticles based on the energy levels.[S6,S7]

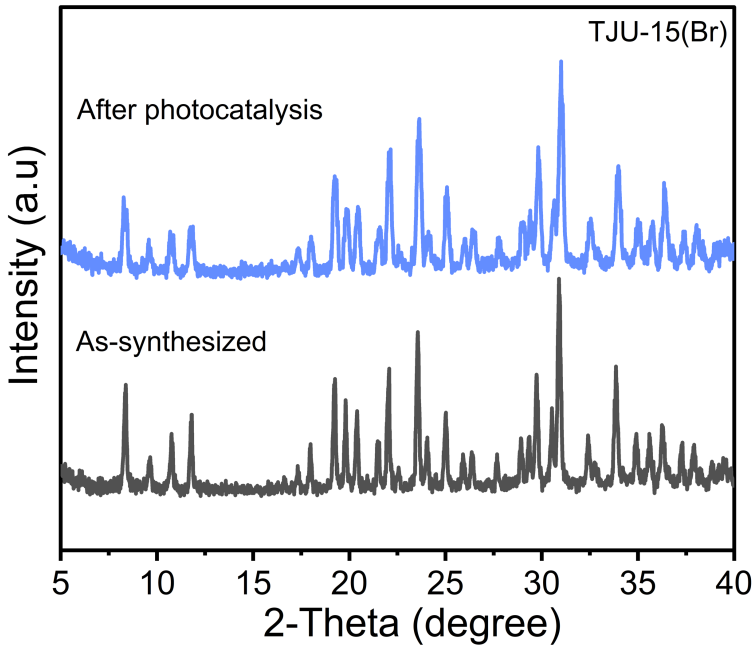

Figure S21. PXRD of $Pt_{0.66}$@TJU-15(Br) before and after five photocatalytic cycles.

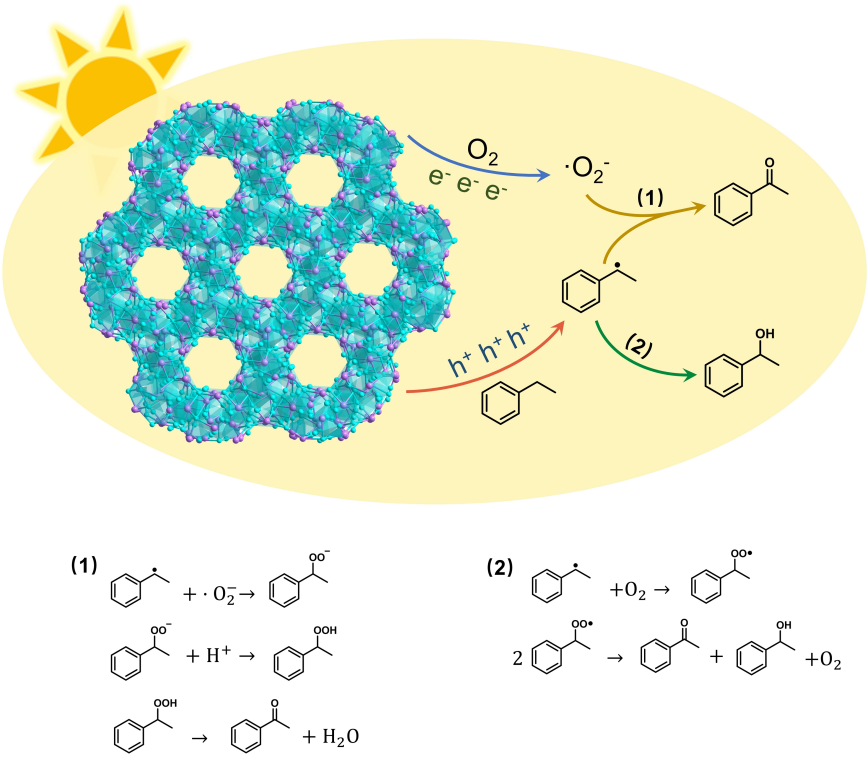

Figure S22. Plausible mechanistic pathway for photocatalytic ethylbenzene oxidation reaction over TJU-15(Br).

Supporing Information References

S1. G. Kresse and J. Furthmüller, *Comp. Mater. Sci.*, 1996, **6**, 15-50.

S2. G. Kresse and D. Joubert, *Phys. Rev. B*, 1999, **59**, 1758-1775.

S3. J. P. Perdew, K. Burke and M. Ernzerhof, *Phys. Rev. Lett.*, 1996, **77**, 3865-3868.

S4. Z. Zhang, Y. Yang, Y. Wang, L. Yang, Q. Li, L. Chen and D. Xu, *Angew. Chem. Int. Ed.*, 2020, **59**, 18136-18139.

S5. H. Huang, H. Yuan, J. Zhao, G. Solís-Fernández, C. Zhou, J. W. Seo, J. Hendrix, E. Debroye, J. A. Steele, J. Hofkens, J. Long and M. B. J. Roeffaers, *ACS Energy Lett.*, 2018, **4**, 203-208.

S6. J.-D. Xiao, Q. Shang, Y. Xiong, Q. Zhang, Y. Luo, S.-H. Yu and H.-L. Jiang, *Angew. Chem. Int. Ed.*, 2016, **55**, 9389-9393.

S7. F. Guo, Y.-P. Wei, S.-Q. Wang, X.-Y. Zhang, F.-M. Wang and W.-Y. Sun, *J. Mater. Chem. A*, 2019, **7**, 26490-26495.